

Chemical dynamics of the reaction $K^*(5p\ 2P) + H_2 \rightarrow KH(v=0;J) + H$: Electronic orbital alignment effects

T.-H. Wong, P. D. Kleiber, and K.-H. Yang

Citation: *The Journal of Chemical Physics* **110**, 6743 (1999); doi: 10.1063/1.478579

View online: <http://dx.doi.org/10.1063/1.478579>

View Table of Contents: <http://scitation.aip.org/content/aip/journal/jcp/110/14?ver=pdfcov>

Published by the [AIP Publishing](#)

Articles you may be interested in

[Angular distributions for the \$F + H_2 \rightarrow HF + H\$ reaction: The role of the F spin-orbit excited state and comparison with molecular beam experiments](#)

J. Chem. Phys. **121**, 5812 (2004); 10.1063/1.1784446

[Quantum and classical studies of the \$O\(3P\) + H_2\(v=0-3, j=0\) \rightarrow OH + H\$ reaction using benchmark potential surfaces](#)

J. Chem. Phys. **120**, 4316 (2004); 10.1063/1.1642580

[State-to-state dynamics of \$H+HD \rightarrow H_2 + D\$ at 0.5 eV: A combined theoretical and experimental study](#)

J. Chem. Phys. **116**, 4769 (2002); 10.1063/1.1461818

[Reaction dynamics of \$Mg\(4s\ 1S, 3s\ 1D\) + H_2\$: Harpoon-type mechanism for highly excited states](#)

J. Chem. Phys. **113**, 5302 (2000); 10.1063/1.1290125

[Energy-dependent cross sections and nonadiabatic reaction dynamics in \$F\(2P_{3/2}, 2P_{1/2}\) + n-H_2 \rightarrow HF\(v,J\) + H\$](#)

J. Chem. Phys. **111**, 8404 (1999); 10.1063/1.480182



Chemical dynamics of the reaction $K^*(5p^2P) + H_2 \rightarrow KH(v=0; J) + H$: Electronic orbital alignment effects

T.-H. Wong^{a)} and P. D. Kleiber^{b)}

Department of Physics and Astronomy, University of Iowa, Iowa City, Iowa 52242

K.-H. Yang

Department of Physics, St. Ambrose University, Davenport, Iowa 52803

(Received 30 October 1998; accepted 12 January 1999)

We report results from scattering state spectroscopic studies of the excited state reaction $K^*(5p^2P) + H_2 \rightarrow KH(v'', J'') + H$. The final state resolved action spectra allow a direct measurement of essential features of the excited state potential surfaces, including regions of local maxima and minima. We observe a pronounced blue-wing–red-wing asymmetry in the reactive to nonreactive branching ratio, peaking in the neighborhood of a strong blue wing satellite. These results show that the dominant reaction pathway passes over a small activation barrier ($350 \pm 100 \text{ cm}^{-1}$) in Σ^+ -like orbital alignment. This result is consistent with an electron jump mechanism through a K^+H^-H ion-pair intermediate. In contrast, approach in Π -like alignment leads predominantly to nonreactive scattering. Our results suggest that a combination of steric and energetic effects determine the major quenching pathways for alkali metal atom- H_2 systems.

© 1999 American Institute of Physics. [S0021-9606(99)00814-4]

I. INTRODUCTION

The reactions of Group I and II excited metal atoms in their “ p ”-states with H_2 to form MH product have been studied for many years.^{1–4} These interactions are useful testing grounds for dynamical models that include nonadiabatic interactions. Depending on the metal atom reagent, two distinct dynamical mechanisms have been identified. One mechanism [as identified in the reaction $Mg^*(3p^1P) + H_2 \rightarrow MgH + H$] involves a surface crossing mechanism in near C_{2v} geometry between the excited $MH_2(1B_2)$ surface and the ground state $1A_1$ surface.^{1–6} The approach to the surface crossing region follows an insertive bond-stretch process where the good molecular orbital overlap in the $1B_2$ state between the metal atom “ p ”-orbital and the σ^* -antibonding orbital of H_2 allows for efficient transfer of electron density, weakening and stretching the H–H bond. In the resulting H–M–H triangular insertion configuration, the ground state ($1A_1$) surface crosses the excited ($1B_2$) surface in a C_{2v} symmetry-allowed crossing seam, which opens a path for efficient quenching to the ground state surface with no significant activation barrier.

Another dynamical pathway for reaction [as identified in the case $Cs^*(7p^2P) + H_2 \rightarrow CsH + H$] is thought to involve an abstractive long-range electron-jump in end-on attack geometry via the repulsive $MH_2(np^2\Sigma^+)$ surface.^{7–9} The reaction proceeds through a crossing of the neutral $M^*(np^2P) + H_2$ potential surface with the ionic M^+H^-H surface, which goes smoothly to the $MH + H$ product valley since the ground state of MH is essentially ionic.^{8,9}

In order to further explore these differing interactions of

excited metal atom “ p ”-states with H_2 , we have used a “half-collision” pump-probe technique to measure the continuum or “scattering state” absorption profiles of the $M-H_2$ collision complex for a number of metal atom reagents.^{5,10–12} The experimental methods have been recently reviewed.¹¹ Essentially the pump-probe experiment involves tuning a laser into the collision broadened line wings of the $M(n'p^2P \leftarrow ns^2S)$ atomic resonance transition to excite the transient collision complex directly in the reactive entrance channel; a second tunable laser then state-selectively probes the nascent branching into distinct product channels. In the Born–Oppenheimer, Franck–Condon approximation, the far wing absorption occurs in a vertical transition between well-defined molecular electronic states of the collision complex. Because the different molecular eigenstates correspond to a particular alignment of the M atom “ p ”-orbital in the collision complex, it is possible to selectively align the reagents, and to study the effect of this alignment on the reaction probability and product energy partitioning. Measurement of the final state resolved absorption profiles (the action spectra) gives information about the shape of the excited state potential energy surfaces (including local extrema), and about the dynamical evolution in the excited state from the Condon point of absorption to the final product state, including insight into both the nuclear motion dynamics and the electronic nonadiabatic interactions which couple the Born–Oppenheimer adiabatic potential surfaces.

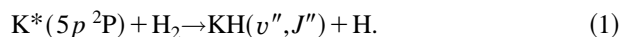
In the case of the reactive quenching of $Na^*(4p^2P)$ by H_2 , our scattering state spectroscopy experiments have shown the presence of two distinct dynamical pathways, one through the attractive “ Π -like” surface and the other on the repulsive “ Σ^+ -like” surface,¹⁵ in agreement with the “insertion” and “abstraction” mechanisms suggested above.^{10,11,13} Our experimental work showed that these dis-

^{a)}Present address: Department of Chemistry, Columbia University, New York, NY 10027.

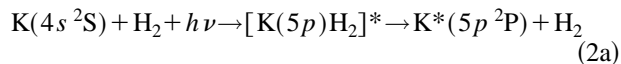
^{b)}Electronic mail: paul-kleiber@uiowa.edu

tinct reaction pathways could be selectively excited by controlling the electronic orbital alignment of the $\text{Na}^*(4p)$ orbital in the transient reaction complex.¹⁰

In order to further clarify the energetic and dynamical effects that control the competitive branching into different reactive and nonreactive quenching pathways we report here the results from spectroscopic studies of the excited state reaction



The kinetics for this reaction have been previously studied.⁹ Our half-collision approach to the study of reaction (1) can be schematically represented



Channel (2a) corresponds to the usual quasielastic collisional absorption process. Channels (2b) and (2c) correspond to the half-collision analog of the nonreactive (E→T,V,R) and reactive collisional quenching processes, respectively.

Our experimental results show that the dominant reaction pathway involves passing over a small barrier ($\sim 350\text{ cm}^{-1}$) in Σ^+ -like alignment, indicative of an abstractive electron jump mechanism through a $\text{K}^+\text{H}^-\text{H}$ ion pair intermediate.⁹ In contrast, approach in Π -like alignment leads predominantly to nonreactive scattering channels. These results are consistent with a suggestion that a combination of steric and energetic factors determine the major quenching pathways for alkali metal atom– H_2 systems.⁸

II. EXPERIMENTAL ARRANGEMENT

The experimental methods have been previously described and only a brief review will be given here.^{5,10,11} A frequency doubled and tripled 30 Hz Nd:YAG laser was used to pump two tunable pulsed dye lasers simultaneously. The pump dye laser was operated with DCM laser dye and sum frequency mixed in a nonlinear mixing crystal to the spectral region near the $\text{K}(5p\ ^2\text{P} \leftarrow 4s\ ^2\text{S})$ second resonance transition at 404.4 nm. The probe dye laser was operated with Coumarin 480 laser dye and tuned into the region of the $\text{KH}(A^1\Sigma^+ \leftarrow X^1\Sigma^+)$ band near 490 nm. The probe dye laser was optically delayed with a delay time of 6 ns. Typical pulse energies were 300 μJ each for the pump and probe dye lasers. The pump laser power varies appreciably over the spectral range and the observed signals are normalized to constant laser power. The two beams were softly focused to a spatial overlap at the center of a heat pipe oven. The oven was operated at a temperature of 500 K, corresponding to a K atom vapor density of $\sim 2 \times 10^{13}/\text{cm}^3$. The oven is filled with H_2 gas a typical operating pressure of 8 Torr.

Branching into the reactive product channels $\text{KH}(v''=0, J''=6 \text{ and } 10)$, corresponding to (2c) above, were measured by laser-induced fluorescence (LIF) on the $A^1\Sigma^+ \leftarrow X^1\Sigma^+$ (7,0) band and detected on the corresponding (7,1) band. The reaction exoergicity from the $\text{K}^*(5p)$ state is $\sim 2900\text{ cm}^{-1}$, so that rotational states up to $J'' \sim 30$ are ener-

getically accessible. However, the KH rotational quantum state distribution is narrowly peaked at low J'' ($J''=6$), with a (full width at half maximum) range from $\sim J''=3$ to $J''=12$. As a result we are unable to probe much higher rotational quantum states. We do have limited data for KH ($v''=0, J''=3$) as well; these results are similar to those presented here for $J''=6$ and 10, but with poorer signal-to-noise owing to the lower initial state population.

The LIF was collected at right angles to the laser axis and focused onto the entrance slit of monochromator. The photomultiplier output signal was collected with a gated integrator interfaced to a personal computer for data acquisition and analysis. A series of experimental linearity tests were performed to verify that the observed LIF signals were linear in incident laser power, H_2 reagent gas pressure, and K atom density, over the range of operating conditions for these experiments.

We have used two separate methods for observing the nonreactive collisional channels in this work. First we measured the direct atomic fluorescence from the laser-excited $\text{K}^*(5p\ ^2\text{P})$ state to the ground state. Narrow spectrometer slits were used to spectrally resolve the collision-induced atomic fluorescence signal from Rayleigh-scattered light due to the off-resonant pump laser. The resulting signals correspond to a measurement of the quasielastic scattering channel (2a). To gain insight into the nonreactive quenching process (2b) we also used the probe laser to detect population in the $\text{K}^*(4p\ ^2\text{P})$ state by laser-induced fluorescence on the $\text{K}(9d\ ^2\text{D} \leftarrow 4p\ ^2\text{P})$ atomic transition. Since the two-step cascade fluorescence process $5p \rightarrow 3d/5s \rightarrow 4p$ is unlikely to be important for the short pump-probe delay time conditions used in these experiments (because of the small $5p \rightarrow 3d/5s$ radiative decay rates), we believe that $4p$ state is predominantly populated through collisional relaxation via the $3d$ intermediate states (*vide infra*).

III. EXPERIMENTAL RESULTS

The main experimental results from this work are presented in Fig. 1, which shows the final state resolved far wing absorption spectra (i.e., the action spectra), corresponding to branching into the different product channels (2) as a function of laser detuning ($\Delta = \omega_L - \omega_0$) in the red and blue wings of the $\text{K}(5p\ ^2\text{P} \leftarrow 4s\ ^2\text{S})$ second resonance transition. Figure 1(a) shows relative population in the nonreactive product channels [corresponding to processes (2a) and (2b)], measured by direct fluorescence from the laser excited $\text{K}^*(5p)$ state, or by probe LIF from the lower lying K atomic $4p$ state as noted above. Figure 1(b) gives the relative populations in the reactive KH ($v''=0, J''=6$ and 10) reactive product channels (2c) measured by probe LIF as discussed. In each case the signals are multiplied by Δ^2 in order to expand the scale and visually enhance the weak far wing signals which arise from the strongest (i.e., smallest impact parameter) collisions.

Pronounced satellites are obvious in the far wing absorption spectra in both the red and blue wings of Fig. 1. Strong satellites are apparent in both the reactive and nonreactive action spectra at $\Delta \sim +250\text{ cm}^{-1}$ in the blue wing and $\Delta \sim -400\text{ cm}^{-1}$ in the red wing. There is also a weak satellite

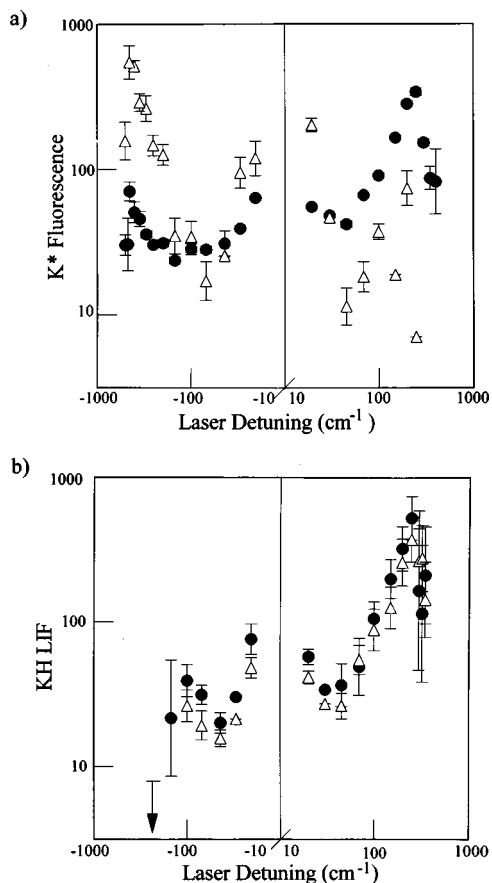


FIG. 1. (a) Nonreactive action spectrum: Log-log plot of the $K^*(5p)$ direct fluorescence (\bullet) and $K^*(4p)$ LIF (Δ), each multiplied by Δ^2 . (b) Reactive action spectrum: Log-log plot of the LIF signals (multiplied by Δ^2) from KH ($v''=0, J''=6$) (\bullet) and KH ($v''=0, J''=10$) (Δ).

feature at $\Delta \sim -100 \text{ cm}^{-1}$ in the near red wing of the reactive action spectrum of Fig. 1(b) {although it is not present in the corresponding nonreactive profile [Figure 1(a)]}. These satellites are analogous to rainbow scattering maxima and result from Franck-Condon excitation into regions of local extrema on the excited state/ground state difference potential energy surfaces.¹¹ We discuss the spectral assignment for the observed satellite features below.

To clarify the chemical dynamics in the $K^*(5p) + \text{H}_2$ collision system, it is useful to consider the relative branching into different quenching channels as a function of detuning in the far line wings. Information about reactive-to-nonreactive product branching is given in Fig. 2 where we have graphed the relative ratio of the observed reactive product KH ($v''=0, J''=6$ and 10) LIF signals to the $K^*(5p)$ direct fluorescence signal (corresponding to the quasielastic scattering channel) in the far-red and blue wings. This is, of course, not the total reactive-to-nonreactive branching since we do not measure all exit channels. Furthermore, due to radiative trapping effects in the direct fluorescence measurement, it is difficult to give a meaningful comparison of the absolute signal levels; thus, the ratio in Fig. 2 is given only as a relative value. Nevertheless, these data do give a clear indication of the reaction pathway.

Note the very strong red-wing-blue-wing asymmetry in

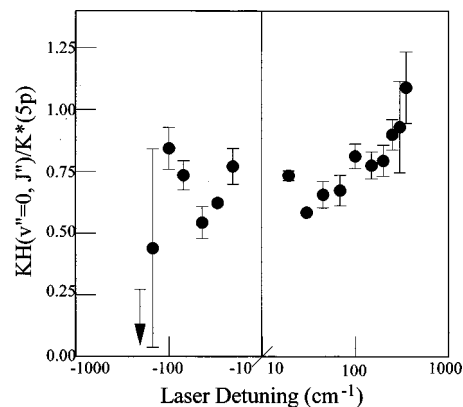


FIG. 2. Reactive to nonreactive branching ratio. The ratio of the KH ($v''=0, J''=6$ and 10) LIF signals to the $K^*(5p)$ direct collisional fluorescence signal, as a function of laser detuning ($\Delta = \omega_L - \omega_0$) in the red and blue wings of the $K(4s-5p)$ resonance line.

the reactive-to-nonreactive branching ratio of Fig. 2. The reactive branching increases rapidly with blue wing detuning and peaks in the region of the blue wing satellite near $\Delta \sim +250 \text{ cm}^{-1}$. Beyond the satellite the total absorption drops sharply. In the red wing, the reactive branching peaks in the region of the near red wing satellite at $\Delta \sim -100 \text{ cm}^{-1}$, and then drops rapidly. Despite a strong overall absorption probability in the far red wing, no reaction product is observed for $\Delta < -150 \text{ cm}^{-1}$. We discuss the dynamical implications of these observations in the next section.

Consideration of the relative branching into the different nonreactive product channels [(2a) and (2b)] is also informative, giving insight into the physical quenching pathways for the $K-\text{H}_2$ system. Figure 3 presents the relative ratio of the probe LIF signal from the $K^*(4p)$ state to the direct collisional fluorescence signal from the $K^*(5p)$ state, as a function of pump laser detuning in the red and blue wings. If the $K^*(4p)$ state were populated primarily through a multistep process involving quasielastic scattering to the $5p$ state [channel (2a)], followed by radiative or collisional relaxation (through subsequent collisions) via the intermediate $5s$ or $3d$ states to the $4p$ state, then the different nonreactive absorption profiles of Fig. 1(a) would be similar and the ratio in

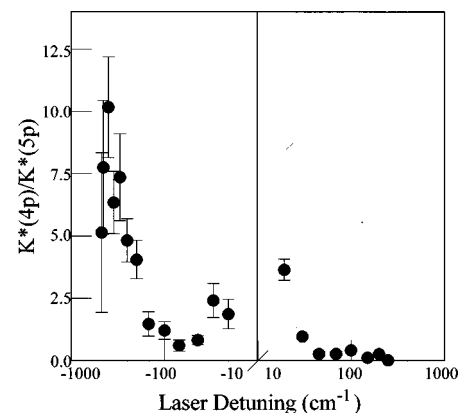


FIG. 3. The ratio of the $K^*(4p)$ laser induced fluorescence signal to the $K^*(5p)$ direct collisional fluorescence signal, as a function of laser detuning ($\Delta = \omega_L - \omega_0$) in the red and blue wings of the $K(4s-5p)$ resonance line.

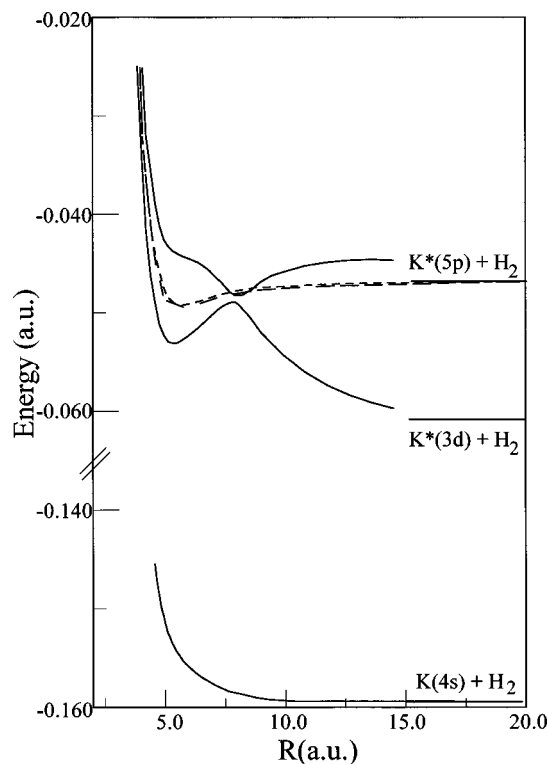
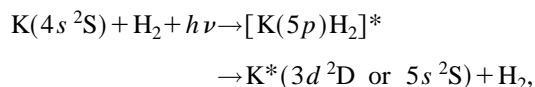


FIG. 4. Relevant potential energy curves for KH_2 . The potentials are for fixed H–H bond length and side-on (C_{2v}) approach geometry: solid lines (2A_1); short dashed lines (2B_1); long dashed lines (2B_2). Adapted from Ref. 14.

Fig. 3 would be essentially flat. However, our experimental design discriminates against such slow multistep processes due to the short pump-probe delay. In fact the clear red-wing–blue-wing asymmetry and structure in the ratio of Fig. 3 shows the effect of direct nonreactive collisional quenching [channel (2b)] in the initial far wing excitation process:



followed by radiative decay (or a second quenching collision) to the $4p$ state. In particular, note the strong resonance peak for nonreactive quenching following excitation in the region of the far red wing satellite near $\Delta \sim -400\text{ cm}^{-1}$, corresponding to a region of the excited state surface which channels flux into the nonreactive quenching channel.

IV. DISCUSSION

Franck–Condon excitation into the spectral region of a far wing satellite corresponds to pumping the transient collision complex directly into the neighborhood of a local extremum on the excited state potential energy surface (accessing a local activation barrier, saddle point, or well). This allows a direct measure of branching into distinct product channels from the transition state region of the excited state surface. Classical satellites are expected based on the pseudopotential calculations of Rossi and Pascale for the $\text{K}+\text{H}_2$ collisional molecule.¹⁴ The Rossi and Pascale potential curves for C_{2v} geometry are reproduced in Fig. 4 for convenience.

The $5p({}^2A_1)\ ^2\Sigma^+$ -like surface shows an obvious local maximum in the potential surface near $\sim 12\text{--}13a_0$. The location is determined in large part by the interaction between the $\text{K}^*(5p)+\text{H}_2$ covalent curve and the K^+-H_2^- ion pair curve which passes through this energy region, and the potential surface maximum represents an activation barrier which must be overcome to access the ion-pair surface crossing region in the proposed electron-jump reaction mechanism. [A similar barrier in the analogous $\text{Na}^*(4p)+\text{H}_2$ system was also found at smaller internuclear distances and higher energies due to the larger ionization potential of Na.¹⁴] Inside this long range barrier the $5p({}^2A_1)\ ^2\Sigma^+$ -like surface shows a deep well, and evidence for an avoided crossing with the lower lying surface of $3d({}^2A_1)\ ^2\Sigma^+$ -like character correlating with the $\text{K}^*(3d)+\text{H}_2$ asymptote.

The attractive Π -like surfaces are anisotropic because molecular orbital overlap determines the degree of bonding interaction. The local minimum in the $5p$ attractive Π -like surface is considerably deeper for C_{2v} approach symmetry than for $C_{\infty v}$ symmetry, as expected for an insertive attack. [Similar results were found for the $\text{Na}-\text{H}_2$ interaction, although in that case the chemical interaction was stronger due to the smaller size of the $\text{Na}(4p)$ atom which allows for more efficient molecular orbital overlap with the σ^* antibonding orbital of H_2 .¹⁴]

To identify the observed spectral features, we have carried out a simple quasistatic lineshape calculation based on the Rossi and Pascale potentials of Fig. 4.^{11,14} The model absorption spectrum predicts a blue wing satellite near $\Delta \sim +550\text{ cm}^{-1}$, correlated with Franck–Condon excitation to the region of the ${}^2\Sigma^+$ -like local surface maximum at long range ($\sim 12\text{--}13a_0$) (Fig. 4). We, therefore, assign the observed blue wing satellite feature near $\Delta \sim +250\text{ cm}^{-1}$ to excitation into this region. The discrepancy in satellite position shows that the pseudopotential calculations significantly overestimate the barrier height in the KH_2 system.

Analysis of the quasistatic lineshapes show that both the ${}^2\Pi$ -like and ${}^2\Sigma^+$ -like surfaces can contribute to the total absorption in the red wing. The model predicts a broad continuum wing resulting from absorption to the attractive $5p$ Π -like surfaces throughout the spectral region of interest. However, red wing excitation to the $5p\ ^2\Sigma^+$ -like surface is also possible inside the long range barrier where the $5p\ ^2\Sigma^+$ -like surface shows a deep well near $\sim 8\text{--}9a_0$. The quasistatic model predicts a satellite near $\Delta \sim -450\text{ cm}^{-1}$, superimposed on the broad absorption continuum. The satellite correlates with Franck–Condon excitation to the inner well region of the $5p\ ^2\Sigma^+$ -like surface. The experimental red wing action spectral satellite observed near $\Delta \sim -400\text{ cm}^{-1}$ can then be assigned to Franck–Condon excitation into region of this potential well on the Σ^+ -like potential energy surface.

However, it is important to realize the real potential energy surfaces in the region from $\sim 7\text{--}9a_0$ are much more complicated than is readily apparent in the restricted geometry curves of Fig. 4. Note that, in C_{2v} geometry (as in $C_{\infty v}$), the $5p({}^2A_1)\ ^2\Sigma^+$ -like surface crosses the attractive $5p({}^2B_1$ and ${}^2B_2)$ Π -like surfaces in the region near the deep minimum at $\sim 8a_0$. However, in the more general (and more probable) C_s approach geometry, the 2B_2 and 2A_1 surfaces

are both of A' character and will show an avoided crossing (conical intersection) leading to an appreciable distortion of the potential energy surfaces in this region. The ${}^2B_1({}^2A'')$ state does not interact and will cross the ${}^2A'$ surfaces. The avoided crossing in A' symmetry can result in a pair of local extrema in the excited state surfaces (i.e., a local minimum in the upper ${}^2A'$ surface and local maximum in the lower ${}^2A'$ surface) which may be evidenced in a broad absorption satellite, or even a pair of absorption satellite features. Thus, the observed satellites near $\Delta \sim -100 \text{ cm}^{-1}$ and $\Delta \sim -400 \text{ cm}^{-1}$ in the red wing may be associated with excitation of a local minimum on the upper ${}^2A'$ surface and a local maximum on the lower ${}^2A'$ surface in the region of the avoided surface crossing in A' symmetry, respectively.

Despite these uncertainties in the details of the potential energy surfaces, we can draw significant and unambiguous conclusions about the quenching dynamics from the experimental data. The strong red-wing–blue-wing asymmetry in the reactive branching of Fig. 2 shows that the reaction occurs exclusively in Σ^+ -like alignment. In contrast, we note that blue wing excitation to the outer wall of the repulsive Σ^+ -like state at long range results primarily in quasielastic scattering and that the probability for direct nonreactive collisional quenching from this region is small. Figures 2 and 3 may be understood in terms of reaction over the long-range barrier on the ${}^2\Sigma^+$ -like potential energy surface. For smaller detunings only the higher energy portion of the Maxwell–Boltzmann velocity distribution has sufficient energy to clear the top of the activation barrier and react, but as the laser is tuned farther up the repulsive wall on the outer side of the barrier, an increasing fraction of the Maxwell–Boltzmann distribution will surmount the barrier.^{10,11} Based on the observed blue wing satellite position we estimate the activation barrier height at $350 \pm 100 \text{ cm}^{-1}$. Note that these experimental techniques allow a direct spectroscopic observation and measurement of the activation barrier. Reaction over an activation barrier in Σ^+ -like orbital alignment is fully consistent with the proposed electron-jump mechanism through a $\text{K}^+\text{H}^-\text{H}$ ion pair intermediate.⁹ This reaction mechanism favors low rotational energy product states as observed. The blue wing action spectra for branching to the different $J'' = 6$ and 10 (and to $J'' = 3$, not shown) are identical to within our experimental uncertainties, consistent with a single reaction pathway.

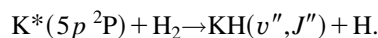
The dramatic decrease in the reactive branching at larger red wing detunings ($\Delta < -100 \text{ cm}^{-1}$) shows that approach in Π -like electronic orbital alignment does not lead to reaction with any significant quantum yield, but rather results predominantly in nonreactive scattering. These observations are in stark contrast with our previous work on the $\text{Na}^*(4p)$ reaction wherein we found competitive branching into both the reactive and nonreactive quenching channels following far red wing absorption.^{10–12} As discussed above, the apparent lack of any reactive quenching pathway through a bond insertion process in the $\text{K}-\text{H}_2$ case might be due to the larger atomic size for K. Because of its larger size, there is less efficient molecular orbital overlap with the small σ^* antibonding orbital of H_2 , and a correspondingly weaker chemical interaction.

Excitation in the region of the near red wing satellite at $\Delta \sim -100 \text{ cm}^{-1}$ probably corresponds to excitation of the local minimum on the upper $5p\ {}^2\Sigma^+$ -like (${}^2A'$) reactive surface above the avoided crossing conical intersection in C_S geometry. Chemical reaction on this surface follows directly by an electron jump mechanism as proposed. This explains why the KH reactive product rotational state branching for excitation in the red wing is identical to that found throughout the blue wing, because the reaction pathway is the same following excitation in both wings. In fact, it is difficult to explain this observation any other way.

Absorption in the region of the red wing satellite near $\Delta \sim -400 \text{ cm}^{-1}$ probably corresponds to direct excitation to the neighborhood of a local maximum on the lower ${}^2A'$ surface below the A' avoided crossing region in C_S symmetry. Excitation in this region shows a strong “resonance” for scattering into the nonreactive quenching channel (Fig. 3). Thus, the surface crossing region near the minimum of the deep $5p\ {}^2\Sigma^+$ -like potential well represents a “hole” in the reactive $5p\ {}^2\Sigma^+$ -like surface that allows for escape or leakage of flux off the reactive surface to a direct nonadiabatic collisional quenching channel to the lower lying ($5s$) or ($3d$) states.

V. SUMMARY

We have reported the results from scattering state spectroscopic studies of the excited state reaction



We observe clear satellite features in both the red and blue spectral wings of the ($5p-4s$) absorption line of the KH_2 collision complex. These spectral features are identified with local extrema on the excited state potential energy surfaces; the observed satellites are in qualitative agreement with the essential surface features predicted in the pseudopotential calculations for KH_2 by Rossi and Pascale.¹⁴ Specifically, a strong blue wing satellite near $\Delta \sim +250 \text{ cm}^{-1}$ is assigned to excitation in the region near a local maximum at long range in the repulsive Σ^+ -like potential energy surface. This potential maximum represents a small (350 cm^{-1}) activation barrier for reaction on the Σ^+ -like surface. We have also observed satellite features in the red wing of the profile and assigned these to excitation into the region of an avoided surface crossing (inside the long range barrier on the Σ^+ -like surface) between the Σ^+ -like and Π -like surfaces in A' symmetry.

We observe a strong blue-wing–red-wing asymmetry in the reactive to nonreactive branching ratio showing that the dominant reaction pathway involves passing over the activation barrier in Σ^+ -like alignment. This result is consistent with an electron jump mechanism through a $\text{K}^+\text{H}^-\text{H}$ ion pair intermediate that has been proposed for this system by Lin and co-workers.⁹ In contrast, approach in Π -like alignment leads predominantly to nonreactive scattering. Experimental evidence also suggests the surface crossing region near the local minimum on the $5p\ {}^2\Sigma^+$ -like reactive surface allows a path for nonreactive quenching to lower lying excited states of K.

These observations are compared with results from previous work on the $\text{Na}^*(4p) + \text{H}_2$ reaction.^{10,11} Clear differences in the experimental observations for the KH_2 and NaH_2 systems suggest that a combination of steric and energetic effects determine the major quenching pathways for alkali metal atom- H_2 systems.⁸

ACKNOWLEDGMENTS

We gratefully acknowledge the support of the National Science Foundation for this work. This manuscript is dedicated to the memory of our colleague and friend, Kenneth M. Sando.

¹W. H. Breckenridge, *J. Phys. Chem.* **100**, 14840 (1996).

²W. H. Breckenridge and H. Umemoto, *J. Chem. Phys.* **80**, 4168 (1984); N. Adams, W. H. Breckenridge, and J. Simons, *Chem. Phys.* **56**, 327 (1981).

³P. Chaquin, A. Sevin, and H. Yu, *J. Phys. Chem.* **89**, 2813 (1985).

⁴K. C. Lin and C. T. Huang, *J. Chem. Phys.* **91**, 5387 (1989); D. K. Liu, T. L. Chin, and K. C. Lin, *Phys. Rev. A* **50**, 4891 (1994).

⁵P. D. Kleiber, A. M. Lyyra, K. M. Sando, V. Zafropulos, and W. C. Stwalley, *J. Chem. Phys.* **85**, 5493 (1986).

⁶L. N. Ding, P. D. Kleiber, M. A. Young, W. C. Stwalley, and A. M. Lyyra, *J. Phys. Chem.* **97**, 2181 (1993).

⁷J. M. L'Hermitte, G. Rahmat, and R. Vetter, *J. Chem. Phys.* **93**, 434 (1990); F. X. Gadea, F. Spiegelmann, M. Pelissier, and J. P. Malrieu, *J. Chem. Phys.* **84**, 4872 (1986).

⁸X. Huang, J. Zhao, G. Xing, X. Wang, and R. Bersohn, *J. Chem. Phys.* **104**, 1338 (1996).

⁹D. K. Liu and K. C. Lin, *J. Chem. Phys.* **105**, 9121 (1996).

¹⁰S. Bililign and P. D. Kleiber, *J. Chem. Phys.* **96**, 213 (1992).

¹¹P. D. Kleiber, in *Chemical Dynamics and Kinetics of Small Radicals*, edited by K. Liu and A. Wagner (World Scientific, Singapore, 1996), p. 573.

¹²P. D. Kleiber, T. H. Wong, and S. Bililign, *J. Chem. Phys.* **98**, 1101 (1993).

¹³A. Sevin and P. Chaquin, *Chem. Phys.* **93**, 49 (1985).

¹⁴F. Rossi and J. Pascale, *Phys. Rev. A* **32**, 2657 (1985).

¹⁵At large M- H_2 distances the internal structure of H_2 may be ignored and the potential surfaces are roughly isotropic and similar to diatomic M-Ne potential curves; for simplicity we use the diatomic state labeling, “ Σ^+ -like” or “ Π -like” to describe the alignment of the M atomic p -orbital parallel or perpendicular to the M- H_2 internuclear axis, respectively.